ontrib Mineral Petrol (1994) 117:263–278

. N. Bindeman · J. C. Bailey

A model of reverse differentiation at Dikii Greben' Volcano, Kamchatka: progressive basic magma vesiculation in a silicic magma chamber

Received: 4 September 1993 / Accepted: 9 March 1994

Abstract Dikii Greben' Volcano is the largest modern volcano with silicic rocks in the Kurile-Kamchatka island arc. It consists of many domes and lava flows of rhyodacite, dacite and andesite which were erupted in a reverse differentiation sequence. Non-equilibrium phenocryst assemblages (quartz + Mg-rich olivine, An-rich + An-poor plagioclase etc.), abundance of chilled mafic pillows in the dacites and andesites, and linear variations of rock compositions in binary plots are considered as mineralogical, textural and geochemical evidence for mixing. Mafic pillows in volcanics have a lower density (because of high porosity) and contain the same non-equilibrium phenocryst assemblages as the host rocks. Their groundmass contains skeletal microlites of plagioclase and amphibole proving that the groundmass as well as the pillows themselves formed from a water-rich basaltic magma at depth. They are considered as supercooled, vesiculated floating drops of a hot hybrid layer in the magma chamber which formed after refilling. The lower density of the inclusions allows them to float in the host magma and to concentrate at the top of the chamber prior to eruption. Magma mingling was effected by mechanical disintegration of the inclusions in the host magma during eruption. The rhyodacitic and basic end-members of the mixing series cannot be linked by low-*P* fractionation though high-*P*, amphibole-rich fractionation is not excluded.

I. N. Bindeman (✉)
Department of the Geophysical Sciences and Enrico Fermi Institute, University of Chicago, 5734 South Ellis Avenue, Chigaco, IL 60637-1433, USA

J. C. Bailey
Division of Petrology, Geology Institute, Copenhagen University, Øster Voldgade 10, DK-1350 Copenhagen K, Denmark

Editorial responsibility: J. Parsons

Introduction

There are many described examples of the contemporaneous association and eruption of a wide variety of magma types in volcanic and plutonic environments (Yoder 1973; Sakuyama 1979; Nixon 1988; Blundy and Sparks 1992) which involve mixing between highly contrasting magmas. Mixing between low-viscosity basic magmas demonstrated in experimental models is considered the usual result of periodic refilling of an evolving magma chamber by new pulses of parental melt (Campbell and Turner 1985; Turner and Campbell 1986). In contrast, fast convective mixing between fluids with large contrasts in viscosity and temperature, e.g. silicic and basic magmas, is practically impossible (Yoder 1973; Turner and Campbell 1986). Petrological studies of some plutons have clearly shown that both basic and silicic magma coexisted in the chamber without extensive mixing throughout much of their evolution (Wiebe 1988, 1993; Litvinovsky et al. 1993).

It is becoming apparent that the most plausible mechanism for mixing magmas with gross differences in composition and temperature is forced convection during eruption (Kouchi and Sunagawa 1985; Koyaguchi and Blake 1989). The calculated short residence time for phenocrysts (Nixon 1988) implies that mixing of different magmas took place shortly before or more likely during the course of eruption. Sakuyama and Koyaguchi (1984) estimated the time necessary for magma mixing as hours/days based on the transportation time for mantle xenoliths. In such time periods, mixing between strongly contrasting magmas is largely incomplete. As the difference in composition and temperature increases, large scale inhomogeneity of compositions and textures appears and sometimes extends to the whole range of compositions between the mixing end-members. For example, quenched mafic inclusions and banded structures in intermediate and silicic rocks are considered to be the result of supercooling and

non-mixing of two thermally constrasting magmas during basic magma refilling of silicic reservoirs (Yoder 1973; Eichelberger 1980). These inhomogeneities along with the mineral zoning pattern record information about the mixing end-members and can be used to estimate the volume proportion of refilling, mixing ratio and mixing history. It should be stressed here that the mixing ratio does not simply reflect the proportions of the two mixing magmas since the mixing history also includes the additional mechanism of basic magma concentration near the chamber roof prior to eruption.

This article is devoted to the petrological study of the active Dikii Greben' Volcano, Kamchatka, which provides an example of large scale mixing between rhyodacitic and basaltic magma which took place in the last 2000–1500 years.

Geology and magmatic evolution of the volcano

The Dikii Greben' (Wild Ridge) Volcano is an active volcano located in south Kamchatka (Fig 1). It is the largest modern volcano with silicic volcanic rocks in the whole Kurile-Kamchatka island arc. The volume of the volcanics exceeds 15 km^3, and these are spread over a territory of about 40 km^2 (Ogorodov et al. 1978). At the present time it is a complex volcanic edifice consisting of a number of extrusive domes and lava flows, accompanied by small amounts of pyroclastic breccias. The main centre of eruption is the highest point of the volcano – Mount Nepriyatnaya (Unpleasant) – which is a partly broken extrusive dome. Large rock falls from Mount Nepriyatnaya occur annually and suggest that the dome may still have been growing until recent times.

The geology and general petrographic features of the volcano are given by Piip (1947), Svyatlovsky (1975), Ogorodov et al. (1978) and Ogorodov (1980).

The Dikii Greben' Volcano series is composed of phenocryst-bearing calc-alkaline rhyodacites (5 km^3), dacites (8 km^3) and andesites (2 km^3). Dacites and andesites, in contrast to rhyodacites, contain mafic pillows (magmatic inclusions) of basaltic and basaltic andesite composition which form a separate mode on the histogram of SiO_2 contents (Fig. 2).

The ^{14}C and tephrochronological age determinations on the volcano reveal the history of eruptions. According to Ogorodov (1980), the basement of the volcano, which is composed of rhyodacitic pumices, has an age of 8000 years. These pumices, which belong to the Kuril'skoye Lake centre and are distinguished from the Dikii Greben' lavas by different K/Na ratios, are not considered further. Some tephrochronologically dated pyroclastic eruptions, also rhyodacitic, took place 5000 and 2000–1500 years ago (Ponomareva, in press). Field observations and tephrochronological data allow us to propose the following sketch of the magmatic evolution. The oldest rocks – rhyodacites lacking magmatic inclusions and forming approximately 30 vol.% of all volcanics – were formed from 8000 until 2000–1500 years ago. They constitute 75–80% of the volcanic history. Dacites and andesites, which form the largest part of the volcanics, were erupted during the last 2000–1500 years and thus take up less than 25–20% of the volcano's history. The magmatic evolution is characterized by reverse differentiation and intensification during the last 2000–1500 years.

Analytical techniques

Minerals were analysed at Moscow State University using an energy dispersive procedure on a CamScan electron microscope with a Link AN1100 microprobe analyser. Major elements in rock samples were obtained by XRF analysis of glass discs at the Chemistry Laboratory of Saratov State University (Table 8) and the Geological Survey of Greenland in Copenhagen (Table 9), supplemented by atomic absorption (Na, Mg) and wet chemical techniques [FeO, H_2O^-, (loss on ignition) LOI]. Most traces were obtained by XRF analysis

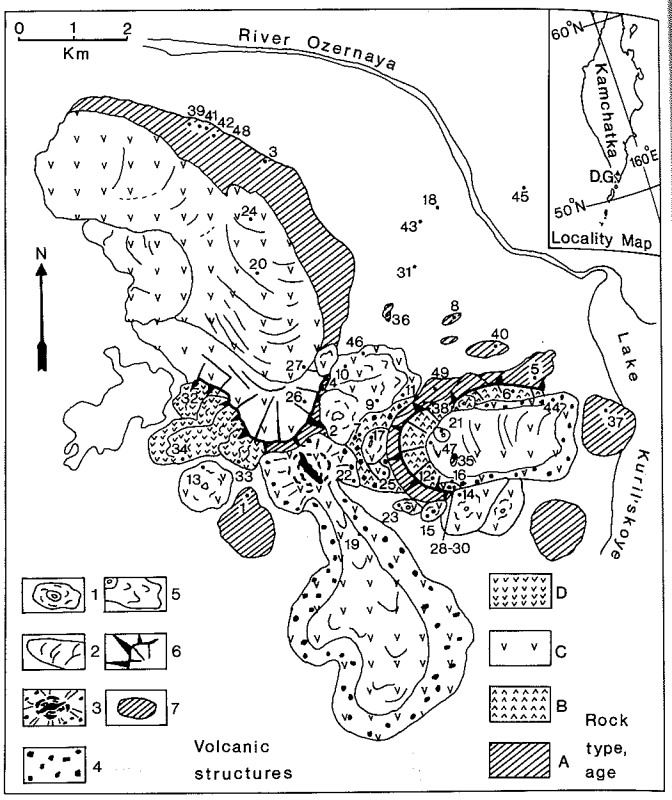

Fig. 1 Geological sketch map of Dikii Greben' Volcano, Kamchatka. Locality numbers correspond to analyses in Table 7. Volcanic structures [extrusive domes, *2* composite extrusive domes, *3* main centre of eruption (Mount Nepriyatnaya) (extrusive dome), *4* deluvial mantles, *5* lava flows, *6* craters, *7* old extrusive domes and lava flows covered by vegetation]. Rock type, age (*A* rhyodacites formed from 8000 to 2000–1500 years; *B–D* rocks formed during the last 2000–1500 years, *B* rhyodacites, *C* dacites, *D* andesites)

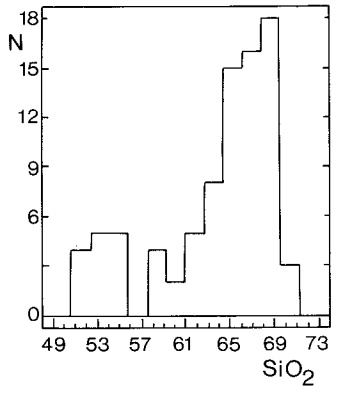

Fig. 2 Frequency histogram for the volcanic rocks and magnetic inclusions from Dikii Greben' Volcano ($N = 86$). Analyses are from Tables 8 and 9, Ogorodov et al. (1978)

(Geology Institute, Copenhagen University) directly on powder pellets using a Philips PW 1400 spectrometer and the techniques of Norrish and Chappell (1977). Cesium REE (rare-earth elements), Th, Hf, Ta, Co and Sc were obtained by INAA (instrumental neutron activation analysis; Tracechem A/S, R. Gwozdz) and U by delayed neutron counting (National Laboratory, Risø). The Sr isotope determinations were made on a VG Sector 54-30 mass spectrometer (Geology Institute, Copenhagen University).

Mineralogy

Phenocryst assemblages

The rhyodacites are coarsely phenocrystal rocks containing idiomorphic and homogeneous plagioclase, quartz, amphibole, orthopyroxene, magnetite, ilmenite and rare biotite (Table 1) set in a glassy groundmass. Dacites and andesites have complex, non-equilibrium phenocryst assemblages: plagioclase, quartz, olivine with chromite inclusions, amphibole, clinopyroxene, orthopyroxene, magnetite and ilmenite. All these phenocrysts are resorbed, and some of them are strongly zoned (normal and reverse) or decomposed (amphibole). The basaltic andesites and basalts occur as mafic pillows, i.e. magmatic inclusions, and have the same phenocryst assemblages as the dacites and andesites. However, the most basic inclusions possess an equilibrium basaltic paragenesis of phenocrysts: olivine, plagioclase, pyroxenes and Fe-Ti oxides (Table 2).

Phenocryst zoning and non-equilibrium phenocryst assemblages

Plagioclase (Pl) phenocrysts form tabular crystals with sizes around 1–5 mm. They have complex zoning from An_{84-30}. According to the zoning pattern, and the composition of phenocryst cores, they can be more or less divided into three types. Type A: phenocrysts with slight normal zoning of the cores from An_{40}–An_{30}. Such compositions, along with crystal morphology and sizes, are similar to those in rhyodacites (Table 1). The zoning of the rims is always reverse, from An_{30} to An_{45}. Type B: phenocrysts with An-rich cores and normal zoning from An_{84} to An_{75} in the centre, identical to plagioclase phenocrysts in basalts (Table 2). Their rims are zoned from An_{75} to An_{45}, like the microlites in inclusions. Type C: the composition and the zoning pattern of the cores of this type are similar to type A, whereas the outer part of the cores often contains a thick (0.3–0.5 mm) "dusty" zone (Fig. 3) surrounded by thin rims with compositions changing from An_{74} to An_{45}. It corresponds to the composition and zoning of microlites in inclusions. The microprobe

Table 1 Representative compositions of phenocrysts in rhyodacites of the Dikii Greben' Volcano *ND* below detection limit, *Pl* plagioclase, *Amph* amphibole, *Opx* orthopyroxene (all Fe as FeO), *Bi* biotite, *Ilm* ilmenite, *Mt* magnetite, *Bulk* bulk composition of the phenocrysts including 1.3 vol.% quartz, *Vol.*% modal amounts of phenocrysts, *An* anorthite, *Or* orthoclase, *Wo* wollastonite, *En* enstatite, *Fs* ferrosilite

	Pl	Amph	Opx	Bi	Ilm	Mt	Bulk
SiO_2	60.66	49.50	54.46	38.01	0.13	0.75	59.28
TiO_2	0.01	1.29	ND	3.94	41.08	6.31	0.34
Al_2O_3	24.92	6.13	0.19	13.95	0.14	1.58	20.26
FeO*	0.17	12.03	21.41	14.23	50.75	78.44	3.68
MnO	ND	0.58	1.52	0.24	0.85	2.25	0.15
MgO	ND	15.05	21.47	15.25	0.12	1.10	2.80
CaO	6.18	10.32	0.88	0.02	0.27	0.55	6.21
Na_2O	7.15	1.47	0.07	1.25	0.28	0.46	5.73
K_2O	0.68	0.43	0.02	8.15	ND	ND	0.71
Cl	ND	0.16	ND	0.33	ND	ND	0.03
Sum	99.77	96.96	100.02	95.37	93.62	91.44	99.19
	An 31 An 65 Or 4		Wo 1 En 66 Fs 33				
Vol.%	25.0	4.5	0.7	0.5		0.5	32.5

Table 2 Representative compositions of phenocrysts in basalts (magmatic inclusions) of the Dikii Greben' Volcano (*ND.* below detection limit; *Ol* olivine, *Sp* spinel, *Cpx* clinopyroxene; pyroxene end-member proportions are based on CaO + MgO + FeO = 100%; FeO* all Fe as FeO)

	Pl	Ol	Sp	Cpx	Opx	Mt	Ilm
SiO_2	43.15	40.01	ND	50.33	55.68	ND	ND
TiO_2	0.03	ND	2.99	0.83	0.22	9.56	40.80
Al_2O_3	34.09	ND	18.65	5.25	0.85	2.45	0.32
FeO*	0.68	17.26	46.94	6.95	15.70	77.43	51.86
MnO	0.05	ND	0.10	0.15	0.21	0.40	0.54
MgO	2.08	42.2	8.99	14.40	26.14	0.82	1.62
CaO	17.04	0.19	ND	20.98	1.47	ND	ND
Na_2O	2.34	ND	ND	0.21	0.05	ND	ND
K_2O	0.35	ND	ND	ND	0.17	ND	ND
NiO	ND	0.22	0.11	0.07	0.02	–	–
Cr_2O_3	ND	0.12	19.64	0.41	0.02	0.49	0.05
V_2O_3	–	–	0.59	–	–	–	–
Sum	99.81	100.00	98.01	99.51	100.53	91.15	95.19
	An 81 Ab 17 Or 2	Fo 81 Fa 19		Wo 40 En 44 Fs 16	Wo 2 En 79 Fs 19		

profile through the "dusty" zone (Fig. 3) shows a non-regular increase of An contents from core to rim. This implies that the dusty zones were formed by partial melting of an initially An poor plagioclase in the course of heating. Compositionally, the various types of plagioclase form a bimodal distribution (not shown) in agreement with their two distinct sources (Sakuyama 1979).

Quartz phenocrysts range from 0.5–3 mm and can be divided into two types. Type A: phenocrysts surrounded by reaction rims of pyroxene. Such quartzes are rounded, small (0.5–1 mm) and abundant in magmatic inclusions. Type B: phenocrysts without reaction rims; they exhibit slightly rounded morphologies and larger sizes (1–3 mm). These crystals are abundant in dacites and andesites, but absent from the inclusions.

Orthopyroxene (Opx) can be divided, according to core compositions and zoning, into three main types. Type A: orthopyroxene with an Fe-rich core $Wo_1En_{66}Fs_{33}$ identical to the one in rhyodacites (Table 1) and slight reverse zoning in the rims to $Wo_3En_{74}Fs_{23}$. Type B: orthopyroxene with an Mg-rich core $Wo_2En_{79}Fs_{19}$, similar to the one in basaltic andesites (Table 2), and normal zoning to $Wo_3En_{74}Fs_{23}$ in the thin rims. Type C: the same as type A but rounded by thin ($\sim 10\mu$), sharply delimited rims with a composition $Wo_3En_{74}Fs_{23}$ identical to microlites in inclusions.

Olivine phenocrysts change in composition from cores with uniform chemical composition Fo_{83} to narrow rims with Fo_{73}. In the inclusions, olivine often forms skeletal phenocrysts which grow from the chilled margins of inclusions towards the centre, indicating fast crystallization (Donaldson 1976). All olivine phenocrysts are rounded by reaction rims of orthopyroxene, augite and pigeonite.

Augite (Cpx) phenocrysts form idiomorphic grains with a uniform chemical composition in the cores, $Wo_{42}En_{43}Fe_{15}$ which is close to the compositions of augite phenocrysts in basalts (Table 2).

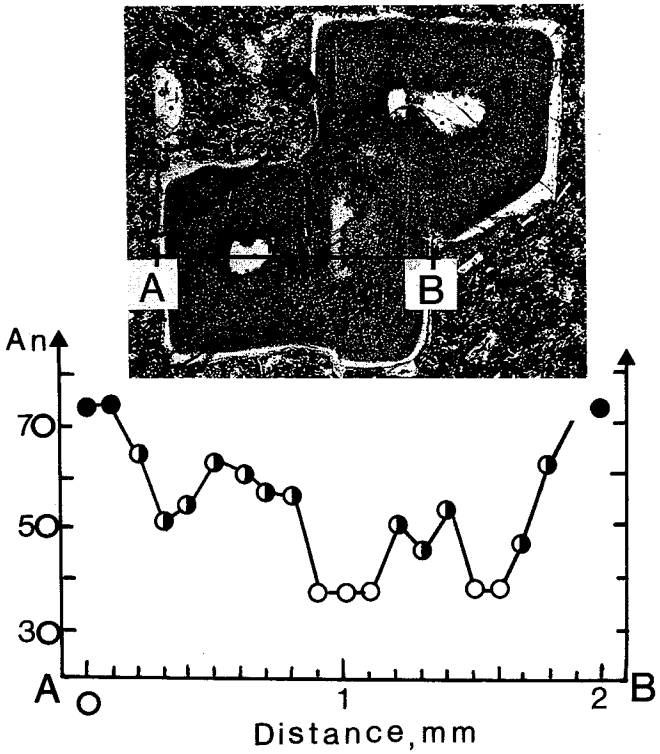

Fig. 3 Plagioclase of "dusty" type in the magmatic inclusions with a microprobe profile through the crystal (*open circles* homogeneous An-poor core, *filled circles* homogeneous An-rich rim, corresponding to microlites, *half-filled circles* "dusty" zone)

The rims are more Fe-rich, $Wo_{33}En_{37}Fs_{20}$ and correspond to the compositions of microlites in inclusions.

Amphibole (Amph) phenocrysts are partly or completely decomposed. In some cases, this process can be explained by the partial dehydration reaction:

$$Amph_1 = Amph_2 + Opx + Cpx + Pl + Magnetite + H_2O$$

In other cases, incongruent melting takes place and small amounts of Al-rich melt (L in Table 3) appear instead of plagioclase.

$$Amph_1 = Amph_2 + Opx + Cpx + L + Magnetite + H_2O$$

The products of these reactions form intergrowths which pseudomorph the original amphiboles. According to Eggler (1972), both these processes indicate heating of the original amphibole. The degree of amphibole decomposition allows a division into two main types of phenocrysts. Type A: partly decomposed amphiboles, characteristic for dacites and andesites but never present in inclusions. Type B: completely decomposed amphiboles occurring in magmatic inclusions. With decreasing SiO_2 contents in rocks and increasing abundance of magmatic inclusions, the ratio of type B/type A amphiboles increases. Both in their morphology and large size, the decomposed amphiboles in dacites and andesites are very similar to those in rhyodacites.

Magnetite and ilmenite are mostly included in mafic phenocrysts and only rarely form independent phenocrysts. Using the composition of coexisting magnetite and ilmenite in an individual phenocryst, we can divide them into two types. Type A: Ti-poor magnetite ($TiO_2 < 7\%$) coexisting with Ti-rich ilmenite ($TiO_2 > 41\%$); these compositions are very similar to the ones in rhyodacites. Type B: Ti-rich magnetite ($TiO_2 > 9\%$) coexisting with Ti-poor ilmenite ($TiO_2 < 41\%$); these phenocrysts are identical to the ones in magmatic inclusions.

Chromite forms rate, resorbed grains which are always together with or included in olivines.

The phenocrysts in magmatic inclusions are identical to those of the host rocks. They can, therefore, be divided into two groups: (1) Phenocrysts, peculiar to the parent magma of the inclusions: olivine with chromite, An-rich plagioclase (type B), magnesian pyroxenes, Ti-rich magnetite and Ti-poor ilmenite. The most basic inclusions contain only these phenocrysts. (2) Phenocrysts captured from the host silicic melt: quartz, An-poor plagioclase, amphibole and Fs-rich orthopyroxene (type C), Ti-poor magnetite and Ti-rich ilmenite. The degree of resorption of these minerals is much higher than in the host rocks.

The described phenocryst assemblages, both in rocks and inclusions, cannot have crystallized in equilibrium with a single melt composition. Their origin is consistent with the mixing of basaltic

Table 3 Incongruent decomposition of amphibole phenocrysts in andesites of the Dikii Greben' Volcano (see text) (*ND* below detection limit, *L* liquid)

	Amph 1	Amph 2	Cpx	Opx	L	Mt
SiO_2	49.78	46.71	49.47	53.66	55.59	ND
TiO_2	1.31	0.77	1.54	0.44	0.08	9.55
Al_2O_3	6.13	9.30	5.06	3.09	23.52	2.02
FeO*	12.02	12.10	10.28	15.31	3.48	77.43
MnO	0.58	0.49	0.31	0.72	0.09	0.40
MgO	15.05	15.16	13.00	23.63	4.04	0.82
CaO	10.32	10.95	19.29	2.97	7.98	ND
Na_2O	1.47	1.57	0.88	0.05	4.34	ND
K_2O	0.62	0.41	0.03	ND	0.65	ND
Sum	97.28	97.46	99.86	99.87	99.77	90.22

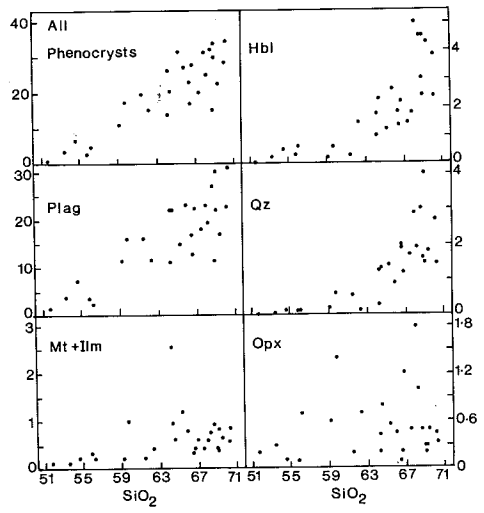

Fig. 4 Variation of phenocrysts contents versus SiO_2 contents (*Hbl* homblende, *Plag* plagioclase, *Qz* quartz, *Mt* magnetite, *Ilm* ilmenite, *Opx* orthopyroxene)

and rhyodacitic magmas with initially different equilibrium phenocryst assemblages: (a) basaltic magma with phenocrysts of olivine, Ca-rich plagioclase, chromite, Mg-rich pyroxenes, Ti-rich magnetite and Ti-poor ilmenite; (b) rhyodacitic magma with phenocrysts of quartz, sodic plagioclase, Fe-rich orthopyroxene, amphibole, Ti-poor magnetite and Ti-rich ilmenite.

Modal amounts of phenocrysts

The modal amounts of phenocrysts change gradually in agreement with the gradual change of bulk rock compositions (Fig. 4). The total phenocryst content, and the amounts of plagioclase, pyroxenes and opaque minerals, show a linear decrease from rhyodacites to basalts (inclusions) along a single trend. The amounts of amphibole and quartz decrease in the same direction but the variations are better described by two trends: subvertical and sloping. The subvertical trend reflects and decreasing volume fraction of amphibole and quartz phenocrysts and implies their dissolution (quartz) or breakdown (amphibole) within the rhyodacitic magma because of heating. In contrast, the recrystallization of plagioclase and pyroxenes is not accompanied by any volume change. The experiments of plagioclase dissolution performed by Watson (1982) and Tsuchuyama (1985) show the formation of reverse and dusty zones while preserving crystal volume and even morphology.

Magmatic inclusions

Magmatic inclusions of basalt and basaltic andesite are abundant as mafic pillows in dacites and especially in andesites. Amounts of inclusions change gradually from 0 (rhyodacites) to 8–12 vol.% in the different volcanic units with different compositions (Fig. 5). The size of inclusions varies widely and was examined statistically in different lava flows and domes. The size distribution of inclusions is always close to lognormal with a maximum in the range 2–5 cm (Fig. 6). The distribution, however, changes its shape between the individual extrusive domes.

The shape of inclusions varies from ellipsoidal to non-regular. Statistical study of the length, width and height of inclusions released from the scoria mantle of one dome indicates that the best

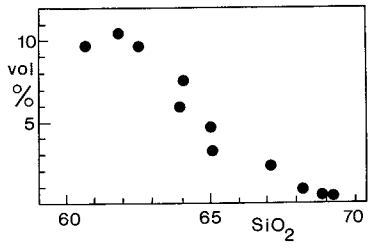

Fig. 5 Volumetric proportion of magmatic inclusions versus SiO_2 contents in the host rocks

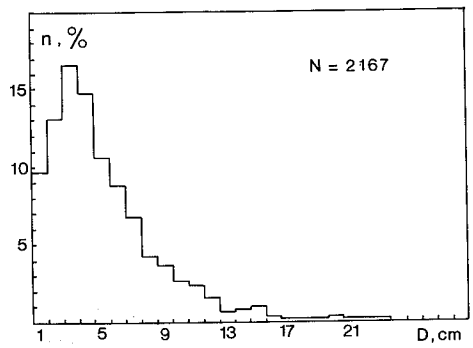

Fig. 6 Distribution of average diameters of magmatic inclusions in rocks of Dikii Greben' Volcano

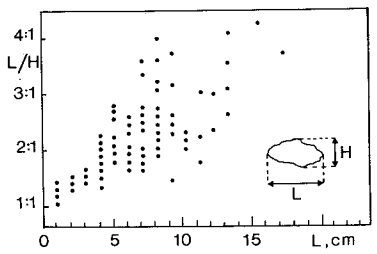

Fig. 7 Prolongation of magmatic inclusions as a function of their length

figure, approximating the inclusions, is the ellipsoid. The ratio length/width for inclusions is greater with increase of the length (Fig. 7). Thus, the largest inclusions have the maximum prolongation.

The texture of inclusions is always strongly porous with 15–20 vol.% of vesicles. This explains the lower densities of inclusions compared to their host rocks (Fig. 8A). Figure 8B shows magmatic densities of 50% crystalline basaltic magma at $T = 1100°C$ and different fluid contents. We see, for example, that basic magma can be less dense than rhyodacitic magma up to 4 km depth if it originally contains 3 wt% water, even if 10 vol.% of amphibole crystallizes in its groundmass. Thus the lower density of inclusions may reflect the inherited porosity of mafic magma due to vesiculation in a magma chamber (Eichelberger 1980).

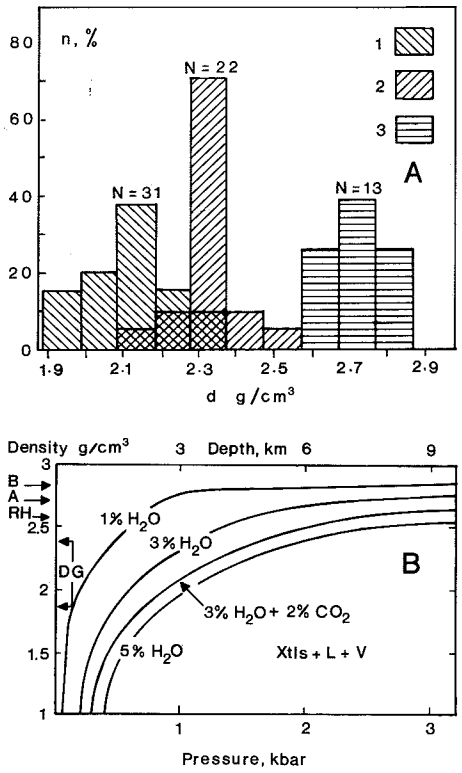

Fig. 8 **A** Statistical comparison between (1) densities of basaltic inclusions and (2) dacites; (3) densities of the powder of basaltic inclusions. **B** Density of basic magma after 50% crystallization at 1100° C and different fluid contents; *P-V-T* data of H_2O are from Burnham et al. (1969) and Fisher (1976), CO_2 are from Shmonov and Shmulovich (1974, 1978). Solubility of water (X, wt%) in subliquids Columbia River basalt is determined through the power law $X = mf^n$ where $m = 1.65$, $n = 0.61$ at 1100° C after experiments of Kadik and Lukanin (1973) and f is water fugacity at the given T and P. Allowance is made for crystallization of 10 vol% of amphibole in the groundmass of inclusions. (*RH*, *A* are densities of non-vesicular rhyodacite and andesite with 3 wt% H_2O and 10% phenocrysts at 2 kbar, *B* is density of dry basaltic magma with 50% crystals at 2 kbar (Bottinga et al. 1982); *DG* is measured densities of magmatic inclusions at Dikii Greben' Volcano)

Groundmass and disintegration of inclusions

Groundmass textures change gradually from rhyodacites through dacites and andesites to basalts (inclusions): the higher the microlite contents in the rocks, the lower the SiO_2 content.

The groundmass of the inclusions has a typical quenched texture with microlites of plagioclase, pyroxenes, amphibole and magnetite plus 20–30 vol.% of interstitial glass. Plagioclase forms hollow crystals in the chilled margins of the inclusions, indicating supercooling of the hot mafic melt (by more than 40° C, Lofgren 1974). However, the central part of the inclusions contains elongated, non-skeletal, even tabular microlites. This proves that cooling proceeded largely from the margins to the centre. The morphology of olivine phenocrysts changes in the same direction: from chain-like at the margins to hollow at the centre. Using the experimental data of Donaldson (1976) on changes in olivine morphology, this indicates variations in the degree of supercooling of the inclusion magma from 80 to 10° under cooling rate conditions of more than 2–20° C/h. Compositions of quenched interstitial glasses are very similar to compositions of host rocks (Table 4). Thus we do not see enrichment

Table 4 Compositions of residual glasses in rocks of Dikii Greben' Volcano

	Basaltic andesites	Andesites	Dacites	Rhyodacites
SiO_2	76.62	77.70	76.48	78.05
TiO_2	0.28	0.39	0.27	0.43
Al_2O_3	12.22	12.05	12.42	11.15
FeO*	1.25	1.18	1.28	1.42
MnO	0.09	0.07	0.07	0.11
MgO	0.27	0.03	0.31	0.05
CaO	1.23	0.61	1.33	0.97
Na_2O	3.16	2.37	2.92	2.12
K_2O	4.61	4.83	4.51	4.88
P_2O_5	0.06	0.07	0.09	0.05
Cl	0.20	0.14	0.30	0.23
Sum	99.99	99.44	99.98	99.46

Table 5 Microlite compositions in andesites and magmatic inclusions, Dikii Greben' Volcano

Mineral	Andesites	Inclusions
Orthopyroxene	Fs_{23}	Fs_{24}
Augite	$Wo_{33}En_{47}Fs_{20}$	$Wo_{35}En_{47}Fs_{28}$
Amphibole	Fe/(Fe + Mg) 27	Fe/(Fe + Mg) 25
Plagioclase	An_{74-40}	An_{75-45}
Magnetite	Present	Present

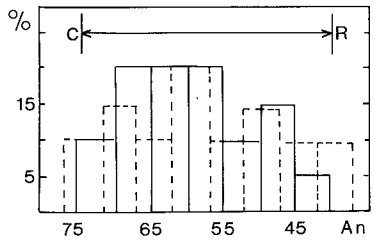

Fig. 9 Statistical comparison between composition of plagioclase microlites in andesites (*solid lines*) and their inclusions (*dashed lines*)

Table 6 Bulk compositions of groundmasses in andesites and inclusions Rock types – see Fig. 1

Rock type	B332 C	B331 C	B306/1 I
SiO_2	60.68	63.15	57.13
TiO_2	1.01	0.86	0.73
Al_2O_3	14.53	14.60	15.65
FeO	8.57	6.65	8.40
MgO	2.95	2.52	4.33
CaO	7.48	5.15	7.49
Na_2O	2.05	3.52	3.49
K_2O	1.30	2.05	0.93
Sum	98.57	98.50	98.15

of the residual melt of the basic magma by components from the host silicic melt as reported for plutonic environments (Blundy and Sparks 1992).

Rhyodacites have a glassy groundmass with small amounts of microlites of amphibole, sodic plagioclase An_{28-30}, orthopyroxene, magnetite and ilmenite.

The paragenesis of the groundmass in dacites and andesites is identical to that in inclusions and is represented by microlites of plagioclase, hypersthene, augite, amphibole, magnetite and by siliceous glass. The morphology, composition and zoning (Table 5, Fig. 9) of minerals in groundmass from rocks with different SiO_2 contents are identical to those in the inclusions. At the same time, the amount of mafic minerals in groundmass of dacites and andesites is 20–30 vol.%, i.e. essentially higher than in the groundmass of typical dacites and andesites in the Kurile-Kamchatka island arc. Thus the bulk composition of groundmasses in andesites and dacites is enriched in Ti, Fe, Ca and K relative to whole-rock compositions at practically the same level of SiO_2. Moreover, the bulk groundmass compositions of andesites are close to the compositions of magmatic inclusions (Table 6). Small (0.2–1 mm) fragments of magmatic inclusions are another important feature of the groundmass textures of dacites and andesites. These observations lead us to conclude that the groundmass of the dacites and andesites was formed by disintegration of microlites and fragments of magmatic inclusions.

Estimation of intensive parameters

To estimate the temperature difference between the rhyodacitic and basic magma before mixing began, we used the two-pyroxene (Wells 1977), plagioclase-melt (Kudo and Weill 1970), olivine-melt (Perchuk 1987), amphibole-plagioclase (Blundy and Holland 1990) and magnetite-ilmenite (Anderson and Lindsley 1985) thermometers for cores of phenocrysts in the most typical rhyodacite (B300) and the most basic inclusion (B306/3). Results of the calculations (Table 7) allow us to conclude that the initial temperature difference between these magmas was about 160° C. In the T-f_{O_2} diagram (Fig. 10), the data points lie along the biotite-amphibole buffer (Carmichael 1967). However, there are two fields of points at 790–820 and ≈ 980° C in agreement with two originally distinct sources for the magnetite and ilmenite phenocrysts which were close to equilibrium with their parental rhyodacitic and basic melts.

The water contents in basaltic magma can be estimated by the methods of Baker and Eggler (1983) and Kadik et al. (1986). Both these approaches are based on consideration of the amphibole stability curve at different degrees of crystallinity. Assuming that amphibole in the magmatic inclusions appeared towards the end of groundmass crystallization, we roughly estimate that it appeared at 50% crystallinity. The curve of 50% crystallinity intersects the amphibole stability curve on the T-X_{H_2O} diagram at about 4–5 wt% H_2O. From this, we infer that the initial H_2O content in the basic magma was about or even more than 4–5 wt%.

Geochemical features of the rocks from the volcano

The rocks from the Dikii Greben' Volcano (Tables 8, 9) belong to a medium-K calc-alkaline series. Harker diagrams for major and trace elements show linear variations (Fig. 11). In particular, FeO* (total Fe as FeO) and TiO_2 trends are not curved and thus differ from trends in many island-arc tholeiitic series where the onset of (or enhanced) crystallization of titanomagnetite is marked by a bend in the variation line (Gill 1981).

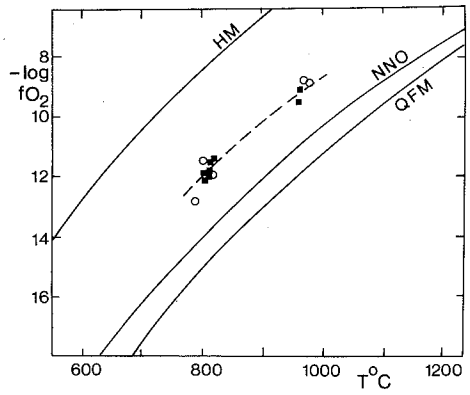

Fig. 10 T-f_{O_2} plot for rocks of Dikii Greben' Volcano (*open circle* rhyodacites, *filled circles* magmatic inclusions, *squares* dacites and andesites, *dashed line* amphibole-biotite buffer of Carmichael, 1967

Table 7 Estimates of temperature difference between rhyodacite and basic magmas

Thermometer	Rhyodacite melt° C	Basalt melt° C	ΔT° C
Olivine-melt (Perchuk 1987)	–	1148–1100	–
Plagioclase-melt (Kudo and Weill 1970)	–	1048	–
Orthopyroxene-clinopyroxene (Wells 1977)	–	1043	–
Amphibole-plagioclase (Blundy and Holland 1990)	790–830	–	–
Magnetite-ilmenite (Andersen and Lindsley 1985)	790–820	980–950	190–130

However, variations of TiO_2, Fe_2O_3, FeO and MgO for some SiO_2-richer magmatic inclusions deviate strongly from the mixing line (Fig. 11) and are better explained by removal of olivine and magnetite phenocrysts.

Log-log diagrams of compatible versus incompatible elements can be used to separate the processes of fractional crystallization (linear trend) from magma mixing (parabolic trend). The Dikii Greben' rocks follow a parabolic trend on a log Ni–log Rb diagram (not

Table 8 Major element analyses of volcanic rocks and inclusions from Dikii Greben' Volcano. Analyses made in Chemistry Laboratory of Saratov State University by X-ray fluorescence spectrometry. Analyses 18–43 are volcanic bombs with age 2000–1500 years and are related to extrusion number 13. Analysis 45 is a volcanic bomb with age 5000 years. Sample numbers of inclusions are sub-numbers of the host volcanic rock. B333/1, B309/1 and B311/1 are inclusions of plagioclase-amphibole dolerite and diroite; the remaining inclusions are fine-grained mafic. Rock types *A*, *B*, *C*, *D* see Fig. 1, *I* inclusions

Sample	B334	B311	B327	B310/1	B300	B301	B309	B323	B313	B310	B314	B318	B333	B319/3	B315
Locality	1 A	2 B	3 A	4 B	5 A	6 B	7 B	8 A	9 C	10 C	11 C	12 B	13 C	14 C	15 C
SiO_2	70.24	69.70	68.96	68.90	68.28	68.28	68.26	68.22	67.76	67.68	67.48	67.32	66.84	66.82	66.62
TiO_2	0.49	0.61	0.56	0.58	0.61	0.58	0.58	0.54	0.56	0.59	0.60	0.64	0.65	0.66	0.63
Al_2O_3	14.12	13.69	14.07	14.54	14.25	14.54	14.54	14.43	14.41	14.39	14.81	15.19	14.86	15.46	15.48
Fe_2O_3	2.88	1.89	1.70	1.48	2.38	1.97	2.20	1.51	2.24	2.69	2.16	3.02	2.22	2.97	2.48
FeO	1.20	2.55	2.12	2.20	2.41	2.20	1.84	2.98	2.91	1.84	2.91	1.91	2.61	2.55	2.55
MnO	0.09	0.08	0.09	0.09	0.10	0.09	0.09	0.10	0.10	0.09	0.10	0.10	0.10	0.11	0.11
MgO	1.33	0.94	1.22	1.53	1.63	1.53	1.74	0.82	2.04	1.63	1.84	1.84	0.71	1.53	2.25
CaO	2.56	3.41	3.41	3.69	3.98	3.55	3.69	4.69	4.12	3.69	3.83	4.12	4.97	4.97	4.40
Na_2O	4.24	4.00	4.20	4.18	4.04	4.26	4.04	3.80	3.72	4.18	3.72	3.72	4.12	3.56	3.64
K_2O	2.19	1.88	2.36	1.93	2.10	1.93	1.93	1.74	1.76	1.93	1.74	1.69	2.29	1.52	1.61
P_2O_5	0.11	0.12	0.15	0.15	0.20	0.15	0.15	0.27	0.20	0.15	0.22	0.25	0.18	0.29	0.25
H_2O^+	1.00	0.72	0.48	0.20	0.30	0.30	0.68	0.70	0.49	0.51	0.25	0.15	0.68	0.00	0.00
Total	100.45	99.59	99.32	99.47	100.28	99.38	99.74	99.80	100.31	99.37	99.66	99.95	100.23	100.44	100.02
	B319/2	B303	B324	B306	B326	B307	B305	B317	B325	B304/1	B330	B329	B319/1	B316	B319/4
	16 C	17 C	18 A	19 C	20 C	21 C	22 C	23 C	24 C	25 A	26 C	27 C	28 C	29 C	30 C
SiO_2	66.44	66.40	66.38	65.88	65.88	65.76	65.50	65.42	65.34	65.26	64.64	64.56	64.30	64.28	64.16
TiO_2	0.64	0.61	0.60	0.70	0.65	0.68	0.73	0.66	0.67	0.67	0.70	0.70	0.66	0.69	0.69
Al_2O_3	15.19	14.66	14.39	14.19	14.72	14.76	14.73	15.18	15.03	15.31	14.82	15.37	15.73	15.16	15.44
Fe_2O_3	3.03	1.56	1.15	3.02	2.30	2.79	2.40	2.48	3.22	1.70	2.00	4.54	4.03	3.75	3.44
FeO	2.34	4.04	4.47	1.99	2.40	2.41	2.84	2.77	3.05	3.40	2.96	1.27	1.28	2.06	2.34
MnO	0.11	0.10	0.10	0.10	0.10	0.10	0.11	0.10	0.12	0.10	0.11	0.12	0.11	0.11	0.12
MgO	1.63	2.04	1.33	2.55	1.63	0.51	2.55	1.74	2.25	2.35	2.45	2.55	1.74	2.45	2.65
CaO	4.97	3.83	4.40	6.32	5.11	7.38	4.40	5.11	4.97	4.54	4.97	4.97	5.54	5.26	4.97
Na_2O	3.72	4.04	3.64	3.78	4.12	3.90	3.90	3.56	3.64	3.90	4.12	4.04	3.64	3.56	3.48
K_2O	1.57	1.83	1.61	1.69	2.12	1.61	1.71	1.57	1.45	1.69	2.12	1.86	1.47	1.40	1.37
P_2O_5	0.29	0.23	0.31	0.22	0.23	0.25	0.25	0.27	0.29	0.25	0.28	0.22	0.25	0.27	0.36
H_2O^+	0.00	0.00	0.85	0.05	0.00	0.04	0.10	0.30	0.24	0.60	0.15	0.23	0.42	0.53	0.20
Total	99.93	99.34	99.23	100.49	99.26	100.19	99.22	99.16	100.27	99.77	99.32	100.43	99.17	99.52	99.22
	B328	B331	B312	B332	B320	C712/1	C828	C834	C823/5	C830	C823/1	C823/2	C712	C829	86603/1
	31 D	32 D	33 D	34 D	35 D	36 A	37 A	38 A	39 A	40 A	41 A	42 A	43 A	44 C	45 A
SiO_2	62.84	62.38	62.14	61.56	59.74	69.53	69.26	68.10	68.92	68.63	68.50	68.39	66.71	65.20	69.48
TiO_2	0.58	0.76	0.73	0.84	0.84	0.37	0.34	0.33	0.32	0.31	0.33	0.37	0.47	0.49	0.36
Al_2O_3	13.79	15.21	15.13	15.84	15.89	14.74	14.41	14.44	14.40	15.10	14.03	14.51	14.67	15.49	14.41
Fe_2O_3	0.16	2.00	3.24	1.01	3.91	1.52	1.31	0.81	1.57	1.98	0.84	1.37	1.60	0.02	3.61
FeO	10.87	4.23	3.62	4.52	3.83	2.30	3.02	4.17	1.87	2.16	3.74	3.06	3.80	5.17	2.01
MnO	0.10	0.11	0.12	0.12	0.13	0.11	0.08	0.08	0.08	0.07	0.09	0.09	0.13	0.11	0.09
MgO	1.33	2.70	3.06	3.47	3.06	1.25	1.25	1.18	1.13	1.36	0.98	1.23	2.35	2.34	0.83
CaO	3.83	5.68	5.82	5.96	7.24	3.89	3.60	3.62	3.40	4.16	3.32	3.74	4.51	5.24	3.80
Na_2O	3.94	3.82	3.40	3.74	3.07	3.92	3.83	3.35	3.70	3.70	4.22	4.09	3.25	3.35	4.38
K_2O	2.12	1.90	1.40	1.69	1.08	2.12	2.26	2.20	2.34	2.21	2.18	2.26	1.90	1.87	2.28
P_2O_5	0.36	0.23	0.31	0.27	0.45	0.07	0.11	0.10	0.09	0.06	0.09	0.03	0.08	0.16	0.02
H_2O^+	0.00	0.60	0.96	0.15	0.25	0.00	0.30	0.17	1.93	0.22	1.37	0.30	0.30	0.52	0.55
Total	99.92	99.62	99.93	99.17	99.49	99.79	99.77	99.55	99.75	99.96	99.69	99.44	99.77	99.96	101.82

Table 8 (continued)

	B306/1	B306/2	B333/1	B306/3	B303/1	B309/1	B311/1	B313/1	B317/1	B319/4	B326/1	C829/1
	19 I	19 I	13 I	19 I	17 I	7 I	2 I	9 I	23 I	14 I	20 I	44 I
SiO_2	5.82	54.80	52.50	51.76	57.94	59.20	52.98	54.66	57.95	53.01	54.23	53.13
TiO_2	0.98	0.97	1.23	1.07	0.89	0.68	1.11	1.01	0.72	0.84	0.75	1.06
Al_2O_3	16.22	16.78	17.82	16.72	16.98	16.35	18.59	17.76	16.48	18.13	17.50	17.85
Fe_2O_3	5.74	6.93	5.04	8.35	4.86	4.44	6.02	5.14	5.21	5.95	7.37	8.45
FeO	2.77	2.06	5.43	2.62	3.45	3.16	4.45	5.03	2.73	4.31	2.87	2.16
MnO	0.14	0.15	0.15	0.10	0.15	0.14	0.17	0.17	0.13	0.16	0.17	0.17
MgO	5.51	5.30	4.49	6.74	2.08	2.18	2.42	2.31	1.92	2.83	2.64	4.56
CaO	7.67	7.95	8.09	7.95	7.62	8.01	9.02	8.42	7.25	10.11	9.58	9.06
Na_2O	3.06	2.96	3.58	2.87	3.80	3.30	3.00	3.00	3.70	2.92	2.92	2.30
K_2O	0.87	0.77	0.87	0.70	1.31	1.55	0.94	1.19	1.48	0.78	0.81	0.81
P_2O_5	0.49	0.48	0.40	0.56	0.27	0.18	0.24	0.25	0.17	0.20	0.17	0.18
H_2O^+	0.00	0.15	0.15	0.47	0.34	0.60	0.75	0.75	1.85	0.43	0.69	2.16
Total	99.77	99.30	99.75	99.91	99.69	99.79	99.69	99.69	99.59	99.67	99.70	101.89

shown) which can be modelled by mixing an evolved, low-Ni basaltic magma with a rhyodacitic magma.

Basaltic inclusions have moderately fractionated REE (rare-earth-element) patterns (Fig. 12) with a persistent, slightly positive Eu anomaly (Eu/Eu* 1.1). In contrast, REE patterns in rhyodacites are markedly more fractionated with higher levels of La and Ce but lower levels of Sm-Lu than in the basalts, and with slightly negative Eu anomalies. Binary mixing of basalt with rhyodacite generates a REE pattern closely matching that of intermediate rocks at Dikii Greben'.

Fractional crystallization in many island-arc series is dominated by low-*P* plagioclase-olivine-pyroxene-magnetite extracts and this process leads to roughly parallel REE patterns with increasing absolute contents throughout the series (Mann 1983; Gerlach et al. 1988). However, Eu anomalies become pronouncedly negative, down to about 0.6. These features are absent in the Dikii Greben' series and effectively rule out the possibility that its basic and acid rocks can be linked by low-*P* fractionation of a single magma.

There are also systematic differences in $^{87}Sr^{86}Sr$ values which exceed our analytical uncertainty: the basic inclusions lie in the narrow range 0.70318–0.70320 whereas dacites and rhyodacites lie at the higher level of 0.70322–0.70330 (Table 10, Fig. 13). Both end-members of the mixing series, however, have ratios similar to basic and acid rocks from other, independent volcanic centres in south Kamchatka.

Geochemical evidence for the sources of the basic and acid end-members of the Dikii Greben' series may now be considered. The basaltic inclusions have the typical incompatible element spectrum of island-arc magmas: compared to MORB (mid-ocean-ridge basalt) they possess positive anomalies for K, Rb, Ba, Sr and Pb but negative anomalies for Zr, Hf, Nb, Ta and Ti. Such a spectrum is thought to be consistent with the partial melting of sub-arc mantle which has suffered metasomatism by fluids released from subducted ocean-floor materials (Gill 1981; Bailey et al. 1989). The $^{87}Sr^{86}Sr$ ratios are consistent with this interpretation.

The source of the acid end-member is more enigmatic. The Dikii Greben' rhyodacites have the geochemical signature of island-arc acid magmas, such as low Ta/Th, Ta/Yb and high Rb/Y + Nb, and are thus unlikely to be the products of crustal melting (Pearce et al. 1984). In addition, they share the same $^{87}Sr^{86}Sr$ values as arc basalts elsewhere in south Kamchatka and could be derived by fractionation of such basalts though, as argued above, not by low-*P* fractionation of the basaltic magma occurring as inclusions at Dikii Greben' Volcano. However, high-*P* fractionation of this basaltic magma, which might be expected to have a high proportion of amphibole in the extract, is an attractive possibility. The presence of amphibole among the phenocrysts of rhyodacites and in the groundmass of basic inclusions is consistent with relatively high water vapour pressures in both magmas. A distinct group of inclusions ranging from microgabbro to microdiorite, and consisting dominantly of plagioclase and amphibole (Table 8: B333/1, B309/1 and B311/1), provide evidence for amphibole crystallization at deeper levels. Their major element features such as high Na/K ratios suggest they are comagmatic with other Dikii Greben' rocks. Slightly enhanced values of TiO_2, FeO*, FeO*/MgO and Al_2O_3 on variation diagrams suggest they represent partial cumulates which are not too distant from liquid compositions. Extensive fractionation of amphibole, which is characterized by high partition coefficients for middle and heavy REE (Green and Pearson 1985), will yield residual liquids with reduced levels of these elements relative to the basaltic parental magma. This is the relationship observed for the Dikii Greben' rhyodacites (Fig. 12). The isotopic data require that this deep-level

Table 9 Selected major and trace element analyses of volcanic rocks and inclusions from Dikii Greben' Volcano. Localities – see Fig. 1; rock types (*I*) magmatic inclusions, *A*, *B*, *C*, *D* See Fig. 1

Locality	44	43	56	43	34	32	44	27	49	7	38
Rock type	I	I	I	I	D	D	C	C	C	B	A
SiO_2	51.92	52.66	53.44	56.41	62.69	63.19	64.52	66.32	67.78	69.08	69.60
TiO_2	0.883	0.810	0.751	0.736	0.647	0.577	0.535	0.521	0.424	0.418	0.374
Al_2O_3	18.81	17.11	16.92	16.21	15.44	15.06	15.42	15.04	15.04	14.47	14.39
Fe_2O_3	9.49	2.98	6.06	3.08	1.41	1.30	3.44	3.82	3.49	0.80	1.80
FeO	0.00	5.18	3.09	4.48	4.52	4.43	1.67	1.01	0.53	2.56	1.48
MnO	0.150	0.146	0.166	0.138	0.124	0.118	0.110	0.114	0.094	0.093	0.088
MgO	4.61	6.39	6.17	5.65	3.07	2.67	2.77	2.40	1.69	1.29	1.41
CaO	10.82	9.53	8.52	8.48	5.70	5.26	5.10	4.79	4.01	3.62	3.40
Na_2O	2.64	2.67	2.67	2.78	3.63	3.66	3.63	3.73	3.99	4.02	3.87
K_2O	0.460	0.940	0.805	1.26	1.81	1.89	1.87	1.95	2.26	2.38	2.42
P_2O_5	0.093	0.188	0.169	0.197	0.165	0.131	0.149	0.142	0.097	0.102	0.053
H_2O^-	0.08	0.22	0.37	0.25	0.46	0.52	0.20	0.25	0.11	0.31	0.21
LOI	0.08	0.46	0.46	0.29	0.26	0.87	0.32	0.10	0.10	0.56	0.58
Total	100.04	99.28	99.59	99.96	99.93	99.68	99.73	100.19	99.62	99.70	99.68
Cs	0.59	0.62	0.55	1.17	1.28	1.36	1.32	1.45	1.28	1.78	1.95
Rb	6.8	15.2	10.1	21.8	32.6	35.6	34.5	35.6	43.2	45.8	47.3
Ba	107	243	281	319	495	532	523	570	627	632	602
Pb	4.5	4.7	7.3	7.1	9.3	10	9.4	9.9	11	11	11
Sr	283	405	364	369	377	350	322	296	283	271	246
K/Rb	560	513	662	480	461	441	450	455	434	431	425
Rb/Sr	0.024	0.038	0.028	0.059	0.086	0.102	0.107	0.120	0.153	0.169	0.192
La	3.2	7.1	7.9	7.5	10.3	10.1	11.0	11.0	10.9	11.4	10.8
Ce	10.5	17.3	17.5	17.9	21.8	21.2	22.2	19.7	22.4	21.8	22.7
Nd	7.5	10.9	10.5	11.7	9.2	10.9	12.2	11.1	10.3	10.1	10.3
Sm	2.30	2.91	2.55	2.73	2.54	2.27	2.62	2.42	2.18	1.89	1.84
Eu	0.95	1.10	0.97	1.03	0.89	0.79	0.82	0.79	0.71	0.64	0.61
Tb	0.57	0.54	0.50	0.48	0.55	0.41	0.48	0.46	0.41	0.34	0.34
Yb	2.27	1.91	1.70	1.85	1.64	1.64	1.72	1.66	1.62	1.25	1.41
Lu	0.34	0.29	0.27	0.27	0.26	0.25	0.26	0.27	0.25	0.22	0.23
Y	22.1	19.9	17.1	18.2	17.4	16.6	17.0	15.9	16.2	13.8	13.5
La/Yb_N [a]	0.93	2.45	3.07	2.68	4.15	4.07	4.22	4.38	4.44	6.02	5.06
Eu/Eu* [b]	1.11	1.11	1.10	1.12	0.98	0.97	0.92	0.95	0.95	1.00	0.97
Th	0.69	0.92	1.10	1.48	2.59	2.75	2.75	2.89	3.40	3.51	3.71
U	0.23	0.33	0.39	0.52	0.94	1.00	1.00	1.08	1.23	1.32	1.38
Zr	52	65	81	76	105	109	109	104	114	122	122
Hf	1.38	1.84	1.95	1.93	2.51	2.54	2.75	2.82	2.83	3.00	2.85
Sn	0.7	1.1	0.8	< 0.5	0.5	0.7	0.5	< 0.5	< 0.5	0.5	0.7
Mo	0.2	0.9	1.3	1.1	1.4	2.2	2.0	1.3	1.1	3.0	2.4
Nb	1.6	2.6	3.8	2.8	3.7	3.7	3.4	4.0	3.3	3.4	3.4
Ta	< 0.11	0.23	0.24	0.18	0.24	0.21	0.24	0.23	0.24	0.25	0.27
Th/U	3.00	2.79	2.82	2.85	2.75	2.75	2.75	2.68	2.76	2.66	2.69
Zr/Hf	38	35	42	39	42	43	40	37	40	41	43
Zr/Nb	33	25	21	27	28	29	32	26	35	36	36
Nb/Ta	–	11	16	16	15	18	14	17	14	14	13
Zn	91	60	78	59	51	51	51	50	39	40	37
Cu	140	13	71	24	36	28	26	26	14	15	6
Co	28	30	33	27	16	14	14	13	8.3	6.9	6.9
Ni	20	45	57	42	22	22	18	13	6	3	5
Sc	40	35	31	32	18	16	16	13	11	8.5	9.0
V	349	250	190	212	144	135	116	109	76	64	70
Cr	55	150	134	139	50	49	30	31	11	12	5.4
As	2.4	0.8	1.2	1.7	2.9	3.6	3.4	4.4	1.5	5.3	4.5
Ga	16	14	16	15	14	13	13	12	14	12	12
Ge	2.0	1.8	1.9	1.6	1.9	1.9	1.5	1.7	1.8	1.7	1.9
S	80	85	5	75	35	75	75	30	50	65	60
Cl	120	210	15	290	200	170	220	100	40	600	480

[a] Chondrite normalized ratio
[b] Europium anomaly

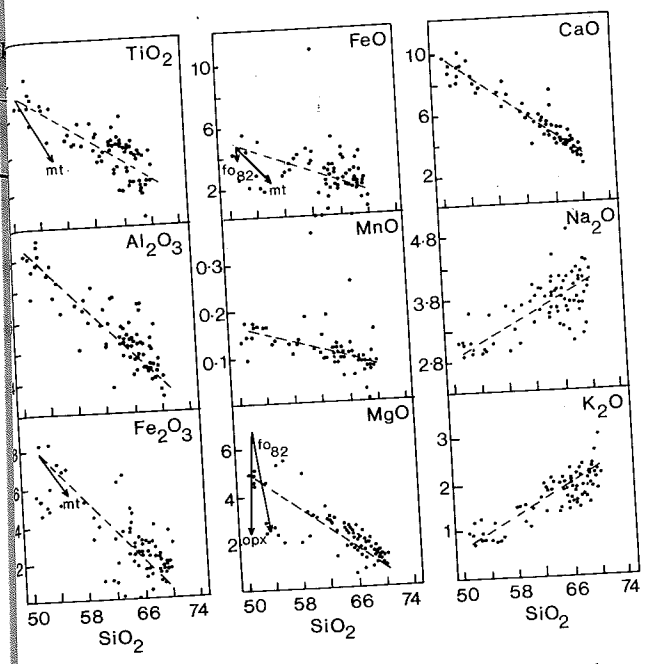

Fig. 11 Harker diagrams for rocks of Dikii Greben' Volcano (*dashed line* mixing line, *arrows* liquid fractionation paths for removal of 5% of magnetite, olivine and orthopyroxene equilibrated with basic magma composition)

fractionation stage is accompanied by a small but systematic increase in $^{87}Sr^{86}Sr$ ratios.

Discussion

The data presented above form the basis for considering the evolution of a shallow magma chamber beneath Dikii Greben' with the long-term presence of an

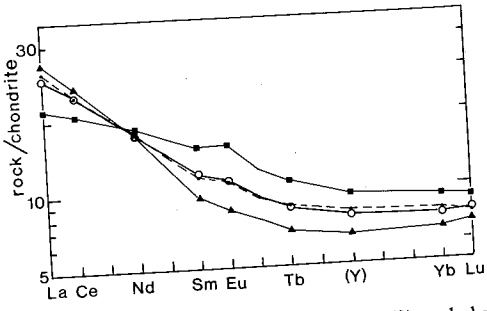

Fig. 12 REE diagram for basaltic (*squares*, C712/9) and rhyodacitic (*triangles*, C834A) samples for Dikii Greben' Volcano. Dacite B331 (*small closed circles*) plots close to a modelled mixture of 0.41 basalt C712/9 and 0.59 rhyodacite C384A (*open circles*)

Table 10 Sr-isotope analyses of volcanic rocks and magmatic inclusions from Dikii Greben' Volcano, Kamchatka. Rock types (*I*-magmatic inclusions; *A*, *C* see Fig. 1)

Sample	Locality	Rock	SiO_2	K_2O	Rb	Sr	$^{87}Sr^{86}Sr$	±
C712/9	43	I	52.66	0.940	15.2	405	0.703201	10
C712/5	46	I	54.70	1.16	18.9	406	0.703182	6
C712/9M	43	I	56.41	1.26	21.8	369	0.703200	11
C713A	46	C	64.41	1.36	23.8	258	0.703301	8
C829	44	C	64.52	1.87	34.5	322	0.703233	11
C712/3	43	C	67.16	2.22	42.6	277	0.703226	6
C833/3	47	C	67.78	2.26	43.2	283	0.703221	7
C830	40	A	68.89	2.33	44.7	266	0.703219	7
C709/6	18	A	68.99	1.68	29.7	185	0.703295	7
C823/4	48	A	69.16	2.48	46.2	247	0.703225	7
C833/1	47	C	69.33	2.32	45.7	258	0.703237	9
C834B	49	A	69.50	2.43	46.9	244	0.703234	7
C834A	49	A	69.60	2.42	47.3	246	0.703224	7

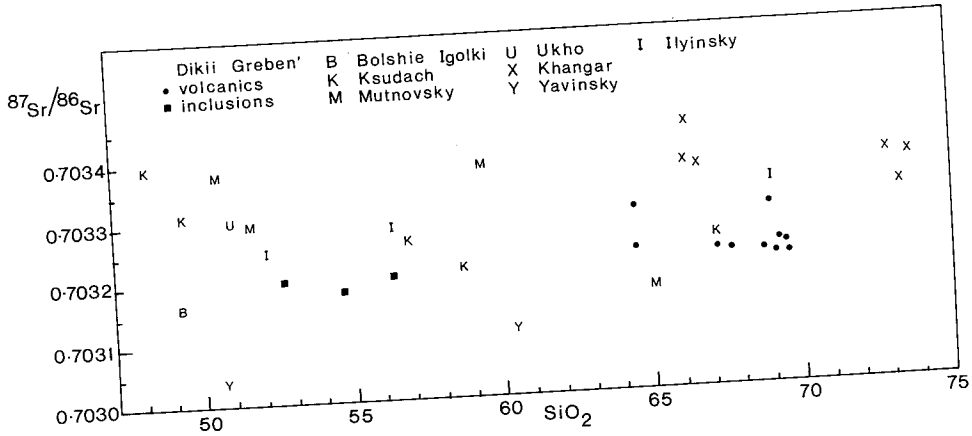

Fig. 13 $^{87}Sr^{86}Sr$ versus SiO_2 for volcanics and basic inclusions from Dikii Greben'. Volcanics from other active island-arc volcanoes in South Kamchatka are shown for comparison. Data sources: Bailey et al. (1987), Volynets et al. (1988) and authors' unpublished data

initially H_2O rich calc-alkaline rhyodacitic melt. This chamber was partly refilled from below by a new pulse of a basic magma. The basic and rhyodacitic magmas cannot be linked through low-*P* fractionation but high-*P* fractionation involving large amounts of amphibole accompanied by slight $^{87}Sr^{86}Sr$ isotopic contamination is not excluded. This suggestion of deep- and shallow-level magma chambers beneath the Dikii Greben' Volcano recalls the petrogenetic model erected for the Tolbachik Volcano (Lukanin et al. 1991). The refilling of the shallow-level chamber by basic magma led to magma mixing and eruption of dacites and andesites with inclusions, and was probably the main factor responsible for the intensification of magmatism during the last 2000–1500 years.

Origin of magmatic inclusions

Although the most basic inclusions have an equilibrium assemblage of basaltic phenocrysts (Table 2), the majority of inclusions possess non-equilibrium phenocryst assemblages suggesting that they are hybrid rocks which record mixing during refilling, residence and/or withdrawal from the magma chamber (Bacon 1986; Koyaguchi 1986). The lower density of the inclusions is the result of their porosity (Fig. 8A) and supports the idea that the inclusions are the product of basic magma vesiculation (Eichelberger 1980). The existence of amphibole in the inclusion groundmasses proves that the groundmass of the inclusions and the inclusions themselves have formed at depths where water vapour pressures were higher than the amphibole stability minimum of 0.5–1.5 kbar (Eggler 1972; Kadik et al. 1986). It also shows that the water content was not less than 4–5 wt%. These conditions allowed the basic magma to become less dense than the overlying rhyodacitic magma in the shallow magma chamber (Fig. 8B). We accordingly view the inclusions as vesiculated supercooled drops of a hot hybrid layer in the magma chamber.

Besides density, the size distribution of the inclusions (Fig. 6) can be taken as evidence for flotation of the inclusions (Bindeman and Podladchikov 1993). The persistent presence of larger inclusions generates a log-normal distribution and may result from their faster flotation (proportional to the square of inclusion radii, according to Stoke's Law) towards the top of the chamber and through the exit channels. A simple calculation shows that, with a viscosity of 10^6 poise for the host rhyodacitic magma, inclusions with radii from 10–25 cm will move upwards 50–300 m a month. This indicates that the flotation of large inclusions is a fast and effective means of transport.

An alternative explanation of the size distribution of inclusions can be given by considering inclusions as a suspension of crystals in a residual melt. Field measurements and theoretical considerations of lava rheology (Pinkerton and Sparks 1978; Pinkerton and Stevenson 1992) show that the behaviour of a partly crystalline basic magma may be understood through Bingham fluid rheology and requires a certain stress value (the yield strength) to initiate motion of such a suspension. Clearly, the effectiveness of inclusion disintegration is strongly dependent on the drag force acting on the surface of an inclusion during flotation (or sinking) through viscous media. Flotation (or sinking) of spherical inclusions of radii less than 1 m in rhyodacitic magma with viscosity $\mu = 10^6$ poise defines a laminar flow regime with Reynolds number < 1. The drag force acting on the surface of the inclusions may be estimated by (Happel and Brenner 1967):

$$F = 6\pi\mu R w$$

where w is the terminal velocity of motion and R is the radii of inclusions. Substituting in this formula the Stokes velocity w:

$$w = \frac{2}{9}\Delta\rho\, g \frac{R^2}{\mu}$$

we obtain:

$$F = \frac{4}{3}\pi\Delta\rho\, g\, R^3$$

where $\Delta\rho$ is the density difference between inclusions and magma and g is the acceleration due to gravity. We can now see that drag force is strongly dependent on the radii of inclusions. This effect is more pronounced if inclusions move through a narrow channel (Happel and Brenner 1967). Yield strength values for 50–70% crystalline basic magma are 600–1500 Pa (recalculated from Pinkerton and Sparks 1978) and will not be exceeded by the drag force acting on the surface of inclusions below 3–5 cm in radius. Large inclusions, however, will disintegrate down to the most stable size of 3–5 cm which is also the most abundant on the distribution plot (Fig. 6).

Figure 7 illustrates the increasing prolongation of the larger inclusions and can be compared with results of experiments on the morphology of liquid drops moving through narrow pipes (Van Dyke 1982). Using these experiments as an analogy, we suggest that inclusion morphology provides a record of magma ascent through a constricted conduit. This, along with the described disintegration, implies that disintegration of the inclusion proceeds due to forced convection during the course of eruption.

The mechanism of magma mixing

It appears that heating or cooling of a multicomponent liquid (magma) can only proceed under non-eutectic

conditions. In the case of Dikii Greben' Volcano, we have established that neither the basic nor the rhyodacitic magma was eutectic (bulk phenocryst compositions differed from bulk rock compositions for both magmas, see Tables 1, 2). On this basis, temperature changes for the contrasting magmas were possible and temperature equilibration was achieved. These processes resulted in heating and mineral dissolution, and crystallization of crystals with reverse zoning in the silicic magma but normal zoning in the basic magma. Apparently, temperature equilibrium between such magmas is achieved prior to any homogenization (Eichelberger 1980; Sparks and Marshall 1986). This is based on the fact that thermal diffusivity coefficients are 4–5 orders of magnitude larger than chemical diffusivities. As a result, two magmas in contact (e.g. inclusions and their host) behave as chemically independent systems during the course of temperature equilibration. At the moment when temperature equilibration is achieved, both magmas attain the same residual melt composition and possess the same composition of phenocryst rims (Fig. 14). At Dikii Greben' Volcano, this conclusion is supported by the similarity in composition of interstitial glasses (Table 4) and phenocryst rims.

Thus, chemical interaction between two thermally equilibrated magmas will not take place because after temperature equilibration both magmas have *already* reached equal compositions of residual melts and phenocryst rims. The former drops of basic magma become inclusions with a much higher degree of crystallinity. Accordingly, the problem of homogenization of the two magmas is one of disintegrating these drops in a common single magma having the same chemical composition. We view this as part of the problem of disintegration of a highly concentrated suspension of rod-like particles.

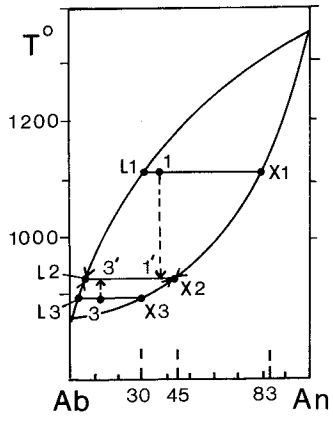

Fig. 14 Results of temperature equilibration between basaltic (1) and rhyodacitic (2) magmas. *l1*, *X1* and *L3*, *X3* are equilibrium compositions of coexisting residual melts and phenocrysts in basaltic and rhyodacitic magmas, respectively. *X1–X2* and *X3–X2* are intervals of normal and reverse zoning detected on phenocrysts (see text). *L1–L2* and *L3–L2* are changes of residual melt composition. (*L2* common single melt composition reached after temperature equilibration, *X2* common single composition of phenocrysts rims. *1–1'* and *3–3'* are paths of temperature equilibration. The form of Ab–An loop is from Johannes (1978) at $P_{H_2O} = 5$ kbar

Many examples of mechanical disintegration of mafic material have been reported from plutonic and volcanic environments (Blundy and Sparks 1992 and references therein). At Dikii Greben' Volcano, statistical comparison of microlite compositions in both inclusions and dome rocks (Fig. 9) suggests that the microlites were formed from the basic magma (inclusions) and then became distributed in the siliceous host. This, along with field observations of mechanical disintegration of inclusions in their host, suggests that the main process of mixing was mechanical disintegration or "micro-dispersion" of the partly solidified supercooled basic drops (inclusions) after their formation. The proportions of these "micro-dispersed" inclusions at various sampled localities changes from 0% for the rhyodacites ($SiO_2 \sim 70\%$) to 45% for the andesites ($SiO_2 \sim 58\%$) and explains the observed diversity of the rocks.

The place and condition of phenocrysts crystallization nd dissolution

The three observed types of phenocrysts reflect different regimes of crystallization-dissolution in the Dikii Greben' magma chamber: weakly reverse zoned phenocrysts of type A are thought to have formed as a result of slight heating of their host rhyodacitic melt; strongly reverse zoned, rimmed phenocrysts of sodic plagioclase, orthopyroxene and quartz with reaction coronas of pyroxenes (type C) are considered to have been incorporated into a hot basic magma layer prior to the mingling which transformed this layer into a hybrid magma; phenocrysts of type B with pronounced normal zoning in rims and skeletal morphology are interpreted to have formed by rapid cooling inside their parental basaltic magma. The trend of fractionation detected in inclusions (Fig. 11) suggests that the process of fractional crystallization of the hot hybrid layer took place throughout its existence beneath the rhyodacitic magma. Thus, the small modal amounts of basic phenocrysts in inclusions (1–3 vol.%) may not be representative of the amounts in the initial basaltic magma. This indicates that inclusions were removed from the upper part of the fractionating basic magma layer.

Types B and C phenocrysts in dacites and andesites have undergone a complicated history. Initially, these phenocrysts were captured by basic magma and were then resorbed. This was followed by rapid cooling because of the formation of inclusions; this is indicated by the unusual basic rims with a high gradient of normal zoning corresponding to the microlites of inclusions. Finally, these phenocrysts were returned into the

host magma by the described process of inclusion disintegration.

Residence time for the basic magma which refilled the silicic magma reservoir

Experimental data on mineral dissolution can be used to estimate the time of dissolution and resorption of different phenocrysts. To form the plagioclase with a dusty zone 0.2 mm wide (Fig. 3) takes 10–1000 years in the temperature range 1125–1000° C and with a diffusion coefficient changing within the experimental error in the range 5×10^{-13}–10^{-14} cm^2/s (Tsuchuyama 1985). The time of dissolution of quartz phenocrysts from an average diameter of 2 mm (rhyolites) to 1 mm (inclusions) using diffusion coefficients varying from 10^{-9}–10^{-11} cm^2/s over the same temperature range (Watson 1982) can be estimated as 0.1–10 years. The lower time obtained using quartz dissolution rates cannot be compared with the plagioclase time, because all quartz phenocrysts in inclusions are rounded by reaction rims of pyroxenes.

The degree of resorption and dissolution of phenocrysts of sodic plagioclase and quartz in inclusions allows us to estimate their residence time in hot basaltic magma, i.e. the time between capture and formation of inclusions. In spite of the present uncertainty in values of diffusion coefficients (Freer 1981) at different temperatures (cf. Tsuchuyama 1985), the estimated times lead us to conclude that the inclusions are not momentarily vesiculated drops of basic magma formed in the course of refilling. Instead, it seems likely that a hot, dense basic magma layer existed for years/decades in the bottom of the chamber.

Mixing scenario

As seen from Fig. 2, most of the hybrid volcanics are represented by dacites (SiO_2 63–68%) and only a small proportion are andesites (SiO_2 58–63%). Using mass-balance calculations, we estimate the proportion of the basic end-member as 0–23 vol.% in dacites and 23–45 vol.% in andesites.

The fact that basic magma forms supercooled inclusions suggests that its proportion is small (cf. Sparks and Marshall 1986). The zoning pattern of minerals in inclusions and in host rocks (Fig. 14) clearly indicates that the final temperature of equilibrium was much closer to the temperature of the colder, silicic melt. Minerals in the host silicic rocks exhibit neither strong resorption nor strong reverse zoning. This leads us to suggest that they were not affected by a large volume of basic magma underlying the silicic one. Intervals of reverse and normal zoning in different minerals and changes of degree of crystallinity of basic and silicic magmas have been used to estimate the proportions of basic magma in a silicic magma chamber (Bindeman 1993). For Dikii Greben' Volcano we estimate that the proportion of the basic magma intruded into the silicic magma reservoir is approximately 5–7 vol.%. However, much more of the basaltic end-member is necessary to produce dacites and especially andesites.

We believe that the proportions of mixing observed in erupted lavas reflect proportions in the exit channels rather than the proportions of mixing in the whole magma chamber. Obvious plutonic examples of this are the high degree of mixing in composite dykes cutting the main body of a pluton with much lower degrees of hybridism (e.g. Litvinovsky et al. 1993). To explain the higher proportion of the basic end-member mingling in the exit channels at Dikii Greben' Volcano, it is necessary that the basic inclusions were concentrated near the chamber roof before eruptions.

We have seen that basic magma remained for some time beneath the rhyodacitic magma and this suggests that it was not dynamically concentrated near the exit channels due to forced injection into the magma chamber. In addition, the possibility of forced withdrawal due to eruption draw-down (Blake and Ivey 1986) seems unlikely; powerful eruptions at Dikii Greben' were absent throughout its life history and could not have disturbed the dense layer of basic magma deep in the stratified reservoir. Furthermore, the inferred small proportion of basic relative to silicic magma makes it difficult to involve the deepest parts of the chamber in the eruptions.

We prefer that the relatively "quiet" mechanism of density inversion of the basic magma layer operated throughout the layer's life. The process of boundary

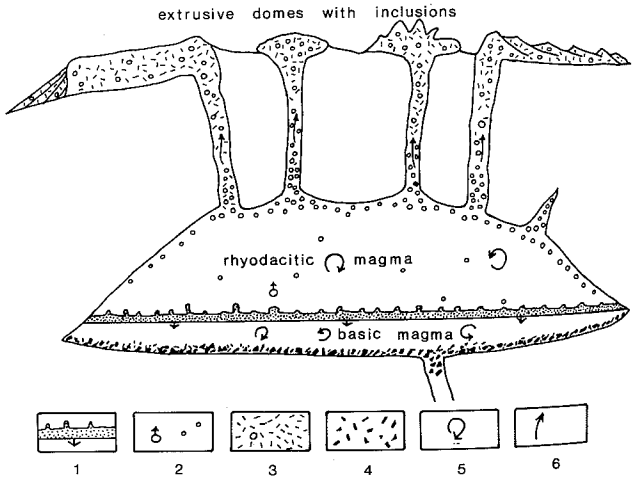

Fig. 15 Inferred magma chamber processes at Dikii Greben' Volcano showing formation of inclusions, their flotation and concentration at the chamber roof, and magma mingling during eruption. *1* front of crystallization and vesiculation, formation of magmatic inclusions and downwards advance of the front, *2* rising magmatic inclusions, *3* mechanically disintegrated inclusions forming hybrid magma, *4* cumulates at the bottom of basic magma layer, *5* convective motion, *6* magma ascent and magma mingling

stallization and vesiculation of the basic magma er would produce rising diapirs which broke up to m basic, vesiculated inclusions capable of floating. ese inclusions would concentrate at the roof and in exit channels (Fig. 15).

Thus, the proportion of magmatic inclusions at ferent moments explains the varying proportions of xing. The reversed differentiation character of volnism at Dikii Greben' Volcano implies that a temral increase of inclusion concentration has taken ace near the chamber's roof.

otation of inclusions and volcanic eruptions

he absence of large pyroclastic eruptions at the Dikii reben' Volcano in spite of the considerable abundce of water suggests the operation of distinctive echanisms of erupting the volcanics and supplying ybrid material to the surface.

Flotation of inclusions with gas bubbles can be onsidered an important factor in the increase of fluid ressure in a magma chamber. This is in accord with he gas-lifting model of Steinberg et al. (1984) and Michaelides (1989). Calculations show that the increase f pressure due to flotation of 3–5 vol.% inclusions is dequate for a slow increase in fluid pressure and this ay lead to periodic, quiet volcanic eruptions in the orm of extrusive domes and lava flows (Bindeman and Podladchikov 1993).

Fluid pressure increase due to flotation of basic nclusions will combine with the continuous process of gas bubble release due to vesiculation of basic magma. These two processes are the energy sources not only for volcanic eruptions but also for the mechanical disintegration (mingling) of basic inclusions in exit channels during eruptions.

Acknowledgements I.N.B. thanks A.Yu. Polukhin and V.L. Sivorotkin for field assistance, and O.N. Volynets and V.V. Ponomareva for helpful discussions and donations of samples. J.C.B. thanks S. Pedersen and P.M. Holm for their guidance in the isotopic work. Jon Blundy and a second referee helped us to clarify and sharpen a number of our arguments. The neutron activation analyses were funded by the Danish Natural Science Research Council (SNF) (J. no. 11-8318).

References

Andersen DJ, Lindsley DH (1985) New (and final!) models for the Ti, magnetite/ilmenite geothermometer and oxygen barometer (abstract). AGU 1985 Spring meet, Eos Trans Am Geophys Union 66 (18):416

Bacon CR (1986) Magmatic inclusions in silicic and intermediate volcanic rocks. J Geophys Res B91 (6):6091–6112

Bailey JC, Larsen O, Frolova TI (1987) Strontium isotope variations in Lower Tertiary–Quaternary volcanic rocks from the Kurile island arc. Contrib Mineral Petrol 95:155–165

Bailey JC, Frolova TI, Burikova IA (1989) Mineralogy, geochemistry and petrogenesis of Kurile island-arc basalts. Contrib Mineral Petrol 102:265–280

Baker DR, Eggler DH (1983) Fractionation path of Atka (Aleutians) high-alumina basalts: Constraints from phase relations. J Volcanol Geotherm Res 18:387–404

Bindeman IN (1993) A practical petrological method for determination of volume proportion of magma chamber refilling. J Volcanol Geothermal Res 56:133–144

Bindeman IN, Podladchikov YuYu (1993) Inclusions in volcanic rocks and a mechanism for triggering volcanic eruptions. Mod Geol 19:1–11

Blake S, Ivey H (1986) Magma mixing and dynamics of withdrawal from the stratified reservoirs. J. Volcanol Geotherm Res 27:153–178

Blundy JD, Holland TJB (1990) Calcic amphibole equilibria and anew amphibole-plagioclase geothermometer. Contrib Mineral Petrol 104:208–224

Blundy JD, Sparks RSJ (1992) Petrogenesis of mafic inclusions in granitoids of the Adamelo massif, Italy. J. Petrol 33:1039–1104

Bottinga Y, Weill DF, Richet P (1982) Density calculations for silicate liquids. I. Revised method for aluminosilicate compositions. Geochim Cosmochim Acta 46:909–919

Burnham CW, Holloway JR, Davis NF (1969) Thermodynamic properties of water to 1,000 degrees C and 10,000 bars. Geol Soc Am Spec Pap 132

Campbell IH, Turner JS (1985) Turbulent mixing between fluids with different vicosities. Nature 313:39–42

Carmichael ISE (1967) The iron-titanium oxides of sodic volcanic rocks and their associated ferromagnesian silicates. Contrib Mineral Petrol 14:36–64

Donaldson CH (1976) An experimental investigation of olivine morphology. Contrib Mineral Petrol 57:187–213

Eggler DH (1972) Amphibole stability in H_2O-undersaturated calcalkaline melts. Earth Planet Sci Lett 15:28–34

Eichelberger JC (1980) Vesiculation of mafic magma during replenishment of silicic magma reservoirs. Nature 288:446–450

Fisher JR (1976) The volumetric properties of H_2O – a graphical portrayal. US Geol Surv J Res 4:189–193

Freer R (1981) Diffusion in silicate minerals and glasses: a data digest and guide to the literature. Contrib. Mineral Petrol 76:440–454

Gerlach DC, Frey FA, Moreno-Roa H, Lopez-Escobar L (1988) Recent volcanism in the Puyehue-Cordon Caulle Region, southern Andes, Chile (40.5° S): petrogenesis of evolved lavas. J. Petrol 29:333–382

Gill JB (1981) Orogenic andesites and plate tectonics. Springer, Berlin Heidelberg New York

Green TH, Pearson NJ (1985) Experimental determination of REE partition coefficients between amphibole and basaltic to andesite liquids at high pressure. Geochim Cosmochim Acta 49:1465–1468

Happel J, Brenner H (1967) Low Reynolds number hydrodynamics with special applications to particulate media. Prentice-Hall, Englewood Cloth, NJ

Johannes W (1978) Melting of plagioclase in the system Ab-An-H_2O and Qz-Ab-An-H_2O at $PH_2O = 5$ kbar, an equilibrium problem. Contrib Mineral Petrol 66:295–303

Kadik AA, Lukanin OA (1973) Behavior of water and carbon dioxide in magmatic processes, governed by their solubility. Geokhimiya 2:163–173

Kadik AA, Maksimov AP, Ivanov BV (1986) Water in magmatic melts (in Russian). Nauka, Moscow

Kouchi A, Sunagawa I (1985) A model for mixing basaltic and dactic magmas as deduced from experimental data. Contrib Mineral Petrol 89:17–23

Koyaguchi T (1986) Evidence for two-state mixing in magmatic inclusions and rhyolitic lava domes on Nijima Island, Japan. J Volcanol Geothermal Res 29:71–98

Koyaguchi T, Blake S (1989) The dynamics of magma mixing in a rising magma batch. Bull Volcanol 52:127–137
Kudo AM, Weill DF (1970) An igneous plagioclase thermometer. Contrib Mineral Petrol 25:52–65
Litvinovsky BA, Zanvilevich AD, Kalmanovich MA, Shadaev MA (1993) Synplutonic basic intrusions of the early stage of formation of the Angaro-Vitim batholith (Transbaikalia) (in Russian). Geol Geophys 33:58–67
Lofgren GE (1974) An experimental study of plagioclase crystal morphology: isothermal crystallization. Am J Sci 274:243–273
Lukanin OA, Kadik AA, Borisov AA (1991) Petrogenesis of the 1975–6 Tolbachik eruption basalts and the origin of high-alumina island-arc basalt magmas. Geokhimiya 1:100–112 (Geochem Int 28, 8:90–101)
Mann AC (1983) Trace element geochemistry of high-alumina basalt-andesite-dacite-rhyodacite lavas of the Main Volcanic Series of Santorini volcano, Greece. Contrib Mineral Petrol 84:43–57
Michaelides EE (1989) The role of vapor in volcanic activity. J Volcanol Geothermal Res 37:251–260
Nixon GT (1988) Petrology of the younger andesites and dacites of Iztaccihuati volcano, Mexico. I. Disequilibrium phenocryst assemblages as indicators of magma chamber processes. J Petrol 29:213–264
Norrish K, Chappel BW (1977) X-ray fluorescence spectrometry. In:Zussman J (ed) Physical methods in determinative mineralogy, 2nd edn. Academic Press, London, pp 201–272
Ogorodov NV (1980) In: Masurenkov VP (ed) Long-lived centre of endogenic activity in south Kamchatka (in Russian) Nauka, Moscow, pp 19–28
Ogorodov NV, Volynets ON, Koloskov AV, Popolitov EI (1978) Dikii Greben' (in Russian). Byull Vulkanol Stn 54:75–88
Pearce JA, Harris NBW, Tindle AG (1984) Trace element discrimination diagrams for the tectonic interpretation of granitic rocks. J Petrol 25:956–983
Perchuk LL (1987) Studies of volcanic series related to the origin of some marginal sea floors. In: Mysen BO (ed) Magmatic processes: physicochemical principles. Geochem Soc Spec Publ 1:209–230
Piip BI (1947) Field geological observations in South Kamchatka (in Russian) Tr Kamchatskoi Vulkanol 3:89–136
Pinkerton H, Sparks RSJ (1978) Field measurements of the rheology of lavas. Nature 276:383–385
Pinkerton H, Stevenson RL (1992) Methods of determining the rheological properties of magmas at subliquids temperatures. J Volcanol Geothermal Res 53:47–66
Ponomareva VV (1994) The largest volcanic explosions in South Kamchatka during Holocene (in Russian). Inst Volcanol Trudi Petropavlovsk (in press)
Sakuyama M (1979) Evidence of magma mixing: petrological study of Shirouma-Oike calc-alkaline andesite volcano, Japan. J Volcanol Geothermal Res 5:179–208
Sakuyama M, Koyaguchi T (1984) Magma mixing in mantle xenolith-bearing calc-alkaline ejecta, Ichinomegata volcano, NE Japan. J Volcanol Geothermal Res 22:199–224
Shmonov VM, Shmulovich KI (1974) Molal volumes and equation of state of CO_2 at temperatures from 100 to 1000 degrees C and pressure from 2000 to 10,000 bars. Acad Sci USSR, Dokl Earth Sci Sect 217:206–209
Shmonov VM, Shmulovich (KI) (1978) Tables of thermodynamic properties of gases and liquids. Series 3. Carbon dioxide (in Russian). Moscow Bur Stand Acad Sci:14–89
Sparks RSJ, Marshall LA (1986) Thermal and mechanical constraints on mixing between mafic and silicic magmas. J Volcanol Geothermal Res 29:99–124
Steinberg GS, Steinberg AS, Merganov AG (1984) Fluid mechanism of pressure increasing in volcanic (magmatic) systems. Dokl USSR Acad Sci 279:886–889
Svyatlovsky AYe (1975) Volcanoes of the USSR (in Russian). Nauka, Moscow
Tsuchiyama A (1985) Dissolution kinetics of plagioclase in the melt of the system diopside-albite-anorthite, and origin of dusty plagioclase in andesite. Contrib Mineral Petrol 89:1–16
Turner JS, Campbell IH (1986) Convection and mixing in magma chambers. Earth-Sci Rev 23:255–352
Van Dyke M (1986) Album of fluid motion. Parabolic Press, Stanford
Volynets ON, Avdeiko GP, Vinogradov VI, Grigor'yeva VS (1988) Sr-isotope zonation in Quaternary lavas of the Kurnile island arc (in Russian). Tikhookeanskaya Geol 1:19–27
Watson B (1982) Basalt contamination by continental crust: some experiments and models. Contrib Mineral Petrol 80:73–87
Wells PRA (1977) Pyroxene thermometry in simple and complex systems. Contrib Mineral Petrol 62:129–139
Wiebe RA (1988) Structural and magmatic evolution of a magma chamber: the Newark Island Layered Intrusion, Nain, Labrador. J Petrol 29:383–411
Wiebe RA (1993) The Pleasant Bay Layered Gabbro-Diorites, Coastal Maine: ponding and crystallization of basaltic injections into silicic magma chamber. J Petrol 34:461–491
Yoder HS (1973) Contemporaneous basaltic and rhyolitic magmas. Am Mineral 58:153–171